Response to Reviewer 1:

This article reports on the effect of OH atmospheric emissions on the retrievals of wind and temperature from the 1.27 μm O_2 dayglow. The topic is very interesting and would deserve publication. However, I have some concern that the authors would need to consider before publishing:

Our reply: We would like to thank the reviewer for his/her overall positive comments and the effort he/she spent on our manuscript.

MAIN CONCERNS:

(1) It is written that "The OH radiance will surely affect the spectral integral intensity of the O_2 emission line near 7823cm^{-1} especially for altitudes between 80 to 90 km where the OH radiance is relatively strong." Given the relative lines intensities, it is difficult to believe that OH contaminate the 1.27 μm O_2 dayglow. Figures 1 and 2 show that OH is not very strong. Therefore, the author should bring more convincing arguments about the need to consider OH.

Our reply: Thank the Referee for the important comment and good suggestion. We have brought more convincing arguments about the need to consider OH dayglow due to its contribution to the increase of wind error and temperature error in the revised manuscript as suggested.

The total spectral irradiance including the weak group of the O_2 dayglow and the OH dayglow is shown in Fig. 3. The third emission line of the O_2 dayglow near 7823 cm^{-1} is too close to the OH lines $RR_{2.5e}$ and $RR_{2.5f}$ (less than 0.05 nm) to be well optically isolated. As can be seen, the OH dayglow affects the observation of the O_2 mission line near 7823 cm^{-1} especially for altitudes between 80 to 90 km where the OH radiance is relatively strong.

The Doppler wavenumber shift in the emission line due to wind velocity is measured as a phase shift of the interferogram, and accurate temperature measurement is determined from the ratio of the integrated absorbances of two isolated emission lines. However, the intensity variation caused by Doppler shift or temperature change is very small. The relative Doppler shift is w/c, where w denotes the motion of the background atmosphere and c is the velocity of light. If winds are to be measured to an accuracy of 3 m/s, a desirable value for the mesosphere and stratosphere, the measurement must be made to one part in 10^8 of the velocity of light. For the central wavelength of 1270 nm, that means the measurement of the wavelength shift is about 12 fm (femtometre). Since a linewidth of the O_2 dayglow is of the order of 0.003 nm, the wavelength shift is 4×10^{-3} of the linewidth. Therefore, the intensity variation of the band radiance near 7823 cm^{-1} caused by the existence of the OH dayglow will surely contribute to the increase of wind error, as well as the temperature error.

(2) The method to compute errors, with and without the knowledge of OH, is not explained in details. It could be useful to describe the method in annex.

Our reply: Thank the Referee for the important comment and good suggestion. We have described the method to compute wind and temperature errors, with and without the knowledge of OH dayglow detailly in the revised manuscript as suggested.

The error standard deviation of inverted wind due to the presence of OH emission is found from the relation

$$\sigma_v = c\ \frac{\sqrt{J_2^2\sigma_{J_3}^2 + J_3^2\sigma_{J_2}^2}}{2\pi\nu_0\Delta(J_2^2 + J_3^2)}$$

Where $\sigma_{J_2}^2$ and $\sigma_{J_3}^2$ represents the variance of the Fourier coefficients J_2 and J_3 due to the lack of knowledge on OH emission.

The error standard deviation of inverted temperature due to the presence of OH emission can be written as

$$\sigma_T = \frac{\Delta T}{T} = \frac{R_{AB}}{T}\frac{dT}{dR_{AB}}\sqrt{\sigma_{J_{1A}}^2 + \sigma_{J_{1B}}^2}$$

Where $\sigma_{J_{1A}}^2$ and $\sigma_{J_{1B}}^2$ represent the variance of the Fourier coefficients J_1 of two emission lines *A* and *B* of the weak group of the O_2 dayglow, and R_{AB} is the ratio of the measured integral absorbances of this two lines, $R_{AB}= J_{1A}/J_{1B}$.

MINOR CONCERNS:

(1) P2L33 two sets of three emission lines. What are the 2 sets exactly?

Our reply: Thank the Reviewer for the very important comment. The two sets of three emission lines mentioned here refer to the weak group and the strong one shown in Fig. 1 of the sixth reference of our manuscript. We have made them clear by referring the corresponding reference in the revised manuscript.

(2) Section 2.1: Is there any auroral excitation of molecular oxygen which can lead to the 1.27 μm emission?

Our reply: Thank the Reviewer for the very important comment. There are auroral enhancements of the infrared atmospheric band emission ($a^1\Delta_g \rightarrow X^3\Sigma_g$) of O_2 near 1.27 μm. The very large aurora1 enhancements in the infrared atmospheric band of O_2 have been reported in the early1970s, such as the rocket measurements of Megill et al. (*J. Geophys. Res.* VOL. 75, 4775, 1970) and the observations by Noxon from an aircraft (*J. Geophys. Res.* VOL. 75, 1879, 1970). More recently, Mertens et al. (*Geophys. Res. Lett.* VOL. 35, L17106, 2008) demonstrated for the first time that $O_2^+ + NO$ charge transfer produces $NO^+(v)$. This mechanism identifies a new source of auroral infrared emission at 4.3 μm, which provides a major step forward in understanding auroral processes and a new context for understanding previously observed auroral enhancements in $O_2(a^1\Delta_g)$ band.

(3) Caption Fig 1: Should not be "Photons" instead of "Photos"?

Our reply: Thank the Referee for careful reading the manuscript and pointing out this problem. We have corrected this mistake in the revised manuscript as suggested.

(4) Figure 2: The caption should say what are the panels a) and b). I assume that a) is O_2 while b) is OH. The caption should explain what the zoom in panel a) is. The X axis of a) and b) should be aligned, such that we see where the overlap between the lines is.

Our reply: Thank the Referee for careful reading the manuscript and pointing out this problem. We have done this in the revised manuscript as suggested. The caption has been said what are the panels and has been explained what the zooms in the panels are. The X axis of a) and b) has been aligned.

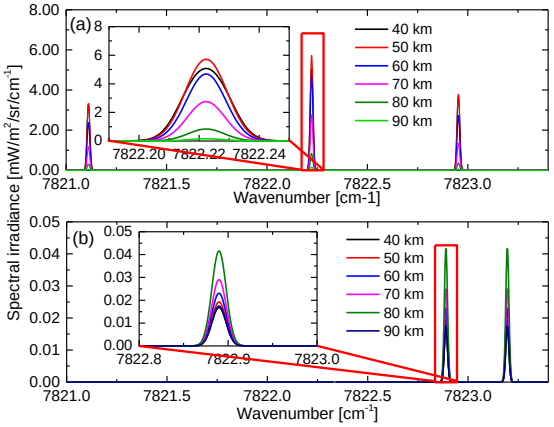

Figure. 2: The spectral irradiance of the three emission lines of O2 dayglow and the two emission lines of OH dayglow at tangent heights of 40 km, 50 km, 60 km, 70 km, 80 km and 90 km. (a) three emission lines of O_2 dayglow. (b) two emission lines of OH dayglow. Inset to (a) or (b) shows a magnified view of a certain emission line of O_2 or OH dayglow, from which the linewidth and intensity varying with tangent heights can see more clearly.

(5) It would be useful to add a plot with: Y axis: Altitude X axis: Ratio between OH and O_2 VER (or radiance), in log scale. In order to see the importance (or not) of the OH lines.

Our reply: Thank the Referee for careful reading the manuscript and pointing out this problem. We have done this in the revised manuscript as suggested (please see Fig. 3(b)).

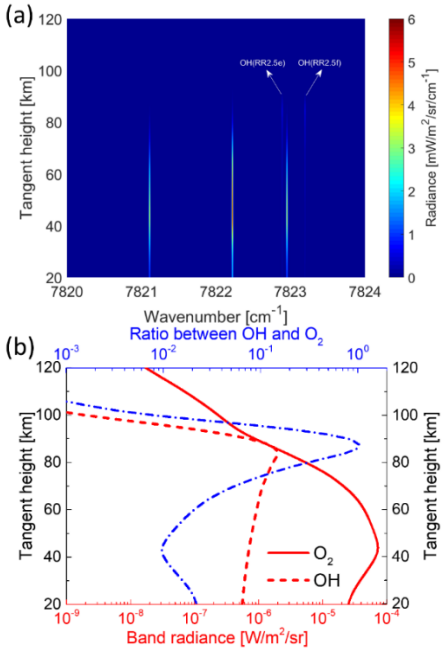

Figure. 3: The total spectral irradiance and band radiance as a function of tangent height. (a) the total spectral irradiance containing $O_2(a^1\Delta_g)$ and OH dayglow as a function of tangent height. (b) the band radiance profiles of the $O_2(a^1\Delta_g)$ and OH dayglow and their ratio.

(6) Figures 6/7: The errors with and without the knowledge of the OH radiance should be drawn in one plot. That will be easier to compare. It is weird not to see the full curve, i.e. around 85 km the scale is too small.

Our reply: Thank the Referee for careful reading the manuscript and pointing out this problem. We have done this in the revised manuscript as suggested (please see Fig. 6).

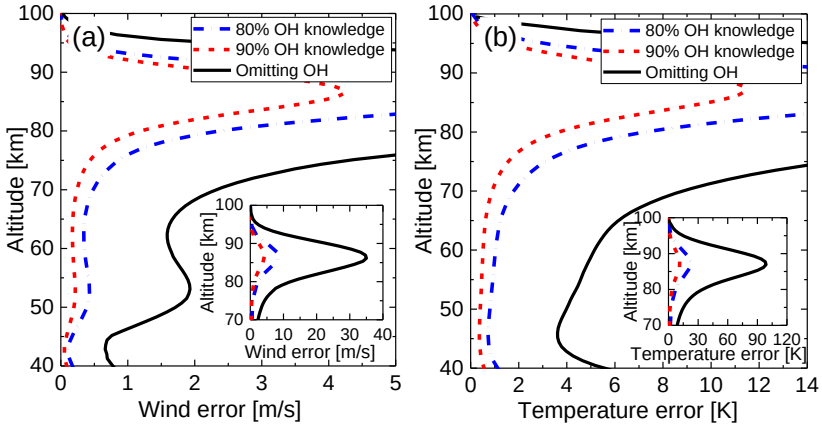

Figure. 6: Inversion errors in wind and temperature due to omitting the presence of OH dayglow (black curve) and with 80% and 90% knowledge of the OH dayglow (blue short dash dot and the red short dash). (a) the wind error profiles. (b) the temperature error profiles. Inset to (a) or (b) shows the wind or temperature error in the altitude range 70-100 km.

Response to Reviewer 2:

Review of Wu O_2 dayglow and OH radiance. This manuscript describes the analysis the authors have made of a proposed new instrument (NWTSI) for the measurement of upper atmospheric wind and temperature, based on an earlier version (WAMI). It deals specifically with a challenge in the design arising from contamination of the primary O_2 emission from the overlapping OH emission and computes the impact of this overlap on the observed winds and temperatures. The rather complex analysis is well done, and the paper is clearly written. However, I have some recommendations with respect to the nomenclature which I have listed under "Overall comments", and others which are minor but need some consideration which I have listed under "Minor comments".

Our reply: Thank the referee for the valuable suggestions and comments that are indispensable in improving the quality of our manuscript.

Overall Comments:

1. I find the units and nomenclature somewhat complicated. For some reason the O_2 is always "O_2 dayglow" and the OH is always "OH radiance" throughout, even though they are the same thing. On line 60 we find "VER" for the first time, without explanation. The volume emission rate (VER) is the number of photons emitted from a cubic centimeter per second (see Figure 1) and is what is most widely used in the field for the airglow. Its integral (photons emitted per

second from a 1 square cm column along the line of sight) is called the "integrated emission rate". Radiance is the column-integrated quantity but in milliwatts per square meter per steradian per cm-1 (wavenumber) (see Figure 2), so is similar but not the same, although it contains almost the same information, except for the spectral range.

Our reply: Thank the Referee for the important comment and good suggestion. We are very sorry for making a mistake of confusing expressions about "dayglow", "radiance", "VER" and "spectral irradiance". We have corrected this incorrect-used terminology and improved the clarity of those sentences including corresponding mistakes in the revised manuscript as suggested.

2. The proposed new instrument contains an "ultra-narrow" filter, described in Line 138: The "ultra-narrow" filter certainly is ultra. The spectral width is not stated, but from the spectral width/free spectral range = 2.0/20 = 0.1 nm. While the fabrication of this filter/etalon is feasible for an highly skilled fabricator, it would be extremely challenging to monitor the changes in its width and central wavelength during the duration of the mission. While this comment is perhaps beyond the scope of this document, the challenge should at least be acknowledged.

Our reply: Thank the Referee for the important comment and good suggestion. We have made this clear in the revised manuscript as suggested. The spectral width of the ultra-narrow filter has been added. And the challenge to monitor the changes in the width and central wavelength of the ultra-narrow filter during the duration of the mission has also been point out.

Minor comments:

1. On line 39, O2(a1D) should have a delta, rather than a "D".

Our reply: Thank the Referee for careful reading the manuscript and pointing out this problem. We have corrected this mistake in the revised manuscript as suggested.

2. On line 47, "will surely contribute" is premature to the analysis, perhaps better to use "may potentially contribute".

Our reply: Thank the Referee for careful reading the manuscript and pointing out this problem. We have corrected this mistake in the revised manuscript as suggested.

3. On line 89 we find "spectral irradiance", shown in Figure 2, which is close to the Integrated Emission Rate.

Our reply: Thank the Referee for careful reading the manuscript and pointing out this problem. In truth, $L(\nu)$ is "spectral irradiance". $L(\nu) = \int_{-\infty}^{\infty} \eta(s) D(\nu, s) \exp[-\int_{-s}^{\infty} n(s')\sigma(s')\,\mathrm{d}s']\,\mathrm{d}s$. Here, the line-shape function of the emission line has been taken into account in this formula. $D(\nu)$ is the Doppler line-shape of a spectral line. The line-shape function $D(\nu)$ is normalized such that $\int D(\nu)\,\mathrm{d}\nu \equiv 1$. Therefore, the unit of $L(\nu)$ is W/m^2/sr/cm^{-1}.

4. On line 95 we find "total radiance", "limb spectral radiance", "O_2 dayglow" and "OH radiance".

Our reply: Thank the Referee for careful reading the manuscript and pointing out this

problem. We have corrected this incorrect-used terminology and improved the clarity of this sentence in the revised manuscript as suggested.

5. Line 96: “too closed” should be “too close”.

Our reply: Thank the Referee for careful reading the manuscript and pointing out this problem. We have corrected this mistake in the revised manuscript as suggested.

6. Line 111: Here the Michelson interferometer is described, but the Optical Path Difference is not given, which is a critical quantity in its design.

Our reply: Thank the Referee for careful reading the manuscript and pointing out this problem. We have given the value of the Optical Path Difference in the revised manuscript as suggested.

7. Line 132: Here we find FPA, but the explanation of it is missing.

Our reply: Thank the Referee for careful reading the manuscript and pointing out this problem. FPA is the short for focal plane array. We have added the explanation of it in the revised manuscript.

8. Line 166: “ring” should be “bring”.

Our reply: Thank the Referee for careful reading the manuscript and pointing out this problem. We have corrected this mistake in the revised manuscript as suggested.

9. Line 173: “closed” should be “close”.

Our reply: Thank the Referee for careful reading the manuscript and pointing out this problem. We have corrected this mistake in the revised manuscript as suggested.

10. Figures 6 and 7. The plots go off scale. Aren’t the off-scale values relevant?

Our reply: Thank the Referee for careful reading the manuscript and pointing out this problem. We have provided new figures in the revised manuscript as suggested (please see Fig. 6).

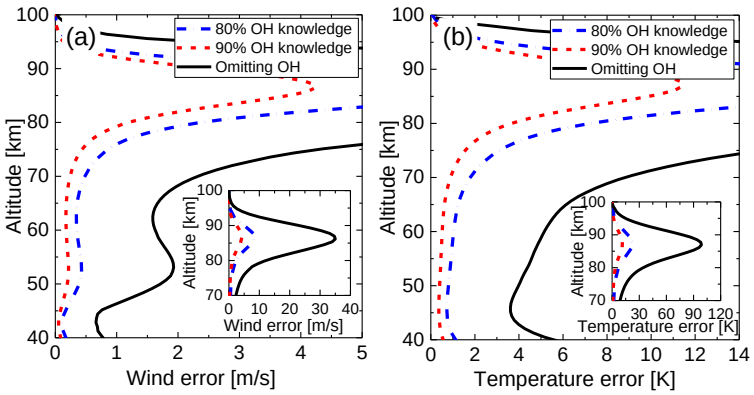

Figure. 6: Inversion errors in wind and temperature due to omitting the presence of OH dayglow (black curve) and with 80% and 90% knowledge of the OH dayglow (blue short dash dot and the red short dash). (a) the wind error profiles. (b) the temperature error profiles. Inset to (a) or (b) shows the wind or temperature error in the altitude range 70-100 km.

Effect of OH radiance on the temperature and wind measurements derived from limb viewing observations of the 1.27 μm O_2 dayglow

Kuijun Wu[1], Weiwei He[2], Yutao Feng[3], Yuanhui Xiong[1], Faquan Li[1]

[1]State Key Laboratory of Magnetic Resonance and Atomic and Molecular Physics, Wuhan Institute of Physics and Mathematics, Chinese Academy of Sciences, Wuhan National Laboratory for Optoelectronics, Wuhan 430071, China.
[2]City College, Wuhan University of Science and Technology, Wuhan, Hubei, 430083, China.
[3]Key Laboratory of Spectral Imaging Technology of Chinese Academy of Sciences, Xi'an Institute of Optics and Precision Mechanics, Chinese Academy of Sciences, Xi'an 710119, China.

Correspondence to: Kuijun Wu (wukuijun@wipm.ac.cn)

Abstract. The $O_2(a^1\Delta_g)$ emission near 1.27 μm is well-suited for remote sensing of global wind and temperature in near-space by limb-viewing observations to its bright signal and extended altitude coverage. However, vibrational-rotational emission lines of the OH dayglow produced by the Hydrogen-Ozone reaction ($H + O_3 \rightarrow OH^* + O_2$) overlap the infrared atmospheric band emission ($a^1\Delta_g \rightarrow X^3\Sigma_g$) of O_2. The main goal of this paper is to discuss the effect of OH radiance on the wind and temperature measurements derived from the 1.27 μm O_2 dayglow limb-viewing observations. The O_2 dayglow and OH radiance spectrum over the spectral region and altitude range of interest is calculated by using the line-by-line radiative transfer model and the most recent photochemical model. The method of four-point sampling of the interferogram and sample results of measurement simulations are provided for both O_2 dayglow and OH radiance. It is apparent from the simulations that the presence of OH radiance as an interfering species decreases the wind and temperature accuracy at all altitudes, but this effect can be reduced obviously by improving OH radiance knowledge.

1 Introduction

The infrared atmospheric band emission ($a^1\Delta_g \rightarrow X^3\Sigma_g$) of O_2 observed near the wavelength of 1.27 μm has remarkable advantages in atmospheric remote sensing due to its bright signal and extended altitude coverage[1]. The enormous success of Wind Imaging Interferometer (WINDII)[2], High Resolution Doppler Imager (HRDI)[3] and TIMED Doppler Interferometer (TIDI)[4], which measured winds in the upper mesosphere and lower thermosphere using Doppler shifts in visible airglow emission lines, stimulates interest in measuring wind and temperature from limb-viewing satellites using the 1.27 μm dayglow[5].

W. E. Ward *et al* designed a high sensitivity interferometer, WAMI, to provide simultaneous measurements of horizontal wind and rotational temperature by using the combination of a "strong" emission lines group and a "weak" group of the $O_2(a^1\Delta_g)$ airglow[6]. A similar instrument, MIMI, designed by York University, also takes advantage of strong and weak emission lines for dynamics and thermodynamics measurement. Both WAMI and MIMI are imaging, field-widened Michelson interferometers and the same measurement technique known as Doppler Michelson imaging interferometry is employed successfully by the WINDII instrument on NASA's UARS satellite[2]. The observing strategy of using two sets of three emission lines (as shown in Fig. 1 of [6]) makes it a perfect approach for WAMI and MIMI to improve our knowledge of the wind and temperature of the lower thermosphere and middle atmosphere, as well as global distribution and transport of O_3. In

recent years, measuring wind and temperature in the planetary atmosphere such as Mars and Venus is also proposed by using 1.27 μm band emission of the electronically excited $O_2(a^1\Delta_g)$ state[7, 8]. Closely following the WAMI concept, we recently proposed a near-space wind and temperature sensing interferometer (NWTSI) for simultaneous measurements of the atmospheric wind and temperature in the near space from the limb-viewing satellite by observing the ~~$O_2(a^1D_g)$~~ $O_2(a^1\Delta_g)$ dayglow near 1.27 μm[9].

The strategy of choosing two sets of three emission lines adopted by WAMI, MIMI and NWTSI is quite ingenious. Three emission lines of each group are relatively well separated and belong to different branches within the same band, which allows them to be optically isolated and ensures distinct temperature sensitivities. Additionally, the line strengths of strong group and the weak one differ by about one order of magnitude, so their radiation intensities and absorption characteristics varying with altitude are available for covering a great extended altitude range from 45 to 100 km.

However, vibrational-rotational emission lines of the OH dayglow produced by the Hydrogen-Ozone reaction ($H + O_3 \rightarrow OH^* + O_2$) overlap the infrared atmospheric band emission ($a^1\Delta_g \rightarrow X^3\Sigma_g$) of O_2 near 1.27 μm[10], which ~~will surely contribute~~ may potentially contribute to the increase of wind and temperature errors.

The main goal of this paper is to discuss the effect of OH radiance on the wind and temperature measurements derived from the 1.27 μm O_2 dayglow limb-viewing observations. The atmospheric radiance model is simulated by line-by-line radiative transfer method. A brief description of O_2 dayglow and OH radiance spectrum over the spectral region and altitude range of interest is provided. The forward simulation including instrument model and the method of four-point sampling of the interferogram, as well as sample results of measurement simulations is presented. Inversion errors of wind and temperature measurements due to the effect of OH radiance are presented and discussed. Here we report, to the best of our knowledge, the first consideration and discussion of the effect of OH radiance on the temperature and wind measurements using the 1.27 μm O_2 dayglow.

2 O_2 and OH dayglow spectrum ~~O_2 dayglow and OH radiance spectrum~~

2.1 The $O_2(a^1\Delta_g)$ and OH dayglow volume emission rates

Two predominant mechanisms, the photolysis of O_3 and the energy transfer from $O(^1D)$, produce the lowest-lying electronic state of molecular oxygen $O_2(a^1\Delta_g)$ in the mesosphere and lower thermosphere. $O_2(a^1\Delta_g)$ radiates strong emission in the infrared atmospheric band $O_2(a^1\Delta_g) \rightarrow O_2(X^3\Sigma_g)$ and produces dayglow at 1.27 μm. The volume emission rate (VER, defined as the number of photons emitted from a cubic centimeter per second) of a O_2 individual rotational line can be given by[11]

$$\eta_{O_2,rot} = A\frac{g'}{Q_{O_2}(T)}\exp\left(\frac{-hcE'}{kT}\right)\frac{\phi_\alpha R_1[O_3] + \sum_{i=1}^{5} K_i[Y_i]\dfrac{[O_2]\left\{R_2 + \phi_\eta R_3[O(^1D)]\right\}}{A_{O_2(b^1\Sigma_g)} + \sum_{i=1}^{5} K_i[Y_i]}}{A_{O_2(a^1\Delta_g)} + \sum_{i=1}^{3} C_i[X_i]} \quad (1)$$

where A is the Einstein coefficient of the transition, g' is the upper state degeneracy, $Q(T)$ is the rotational partition function, h is the Planck constant, c is the light speed, and k is the Boltzmann constant, T is the rotational temperature, E' is the upper state energy, $X = \{O_2, N_2, O\}$, $Y = \{N_2, O_2, CO_2, O_3, O\}$, $R_1 = 8.1\times10^{-3}$, $R_2 = 5.35\times10^{-9}$, $R_3 = 3.2\times10^{-11}\exp(70/T)$ $C_1 = 3.6\times10^{-18}e^{-220/T}$, $C_2 = 1.0\times10^{-20}$, $C_3 = 1.3\times10^{-16}$, $K_1 = 2.1\times10^{-15}$, $K_2 = 4.2\times10^{-13}$, $K_3 = 2.2\times10^{-11}$, $K_4 = 8.0\times10^{-14}$ and $K_5 = 3.9\times10^{-17}$, $0.54 < \phi_\eta < 1.0$.

An enhanced concentration of OH* in high states occurs in a thin layer near the mesopause due to the Hydrogen-Ozone reaction, $H + O_3 \rightarrow OH^* + O_2$. A multitude of excited OH* in high vibrational and rotational states cascading to lower energy states results in an emission spectrum, which extends over a wide wavelength range (500–5000 nm). Among those vibrational-rotational transitions, two emission lines, $RR_{2.5e}$ and $RR_{2.5f}$ of the $OH(X\,^2\Pi_{3/2}, \upsilon' = 8) \rightarrow OH(X\,^2\Pi_{3/2}, \upsilon'' = 5)$ band, are very close to the three weak target emission lines of the 1.27 μm O_2 dayglow.

The volume emission rate of the OH (8–5) vibrational band can be given by[12]

$$\eta_{OH,8-5}(J', J'') = 2(2J'+1)\frac{[\mathrm{OH}(v=8)]A_{8-5}^{J',J''}}{Q_{OH}(\mathrm{T})}\exp(-\frac{hcF_{8-5}(J')}{kT}) \quad (2)$$

where $[\mathrm{OH}(v=8)]$ is the number density of OH in the $v=8$ state, $A_{8-5}^{J',J''}$ is the particular Einstein coefficient for the rotation transition of the (8–5) vibrational band, J' and J'' are initial and final values of the total angular momentum of the transition, $F_{8-5}(J')$ is the upper state rotational term value.

Figure 1 shows the VER profiles of both the three weak target emission lines of the 1.27 μm O_2 dayglow and the two emission lines, $RR_{2.5e}$ and $RR_{2.5f}$ of the $OH(X\,^2\Pi_{3/2}, \upsilon' = 8) \rightarrow OH(X\,^2\Pi_{3/2}, \upsilon'' = 5)$ band. As can be seen, the O_2 dayglow peaks at about 45 km and the OH reaches 90 km, and the emission rate of O_2 is roughly 45 times stronger than OH. In addition, the two emission lines of OH show a similar distribution profile over altitude, while, the three emission lines of O_2 differs a lot. This is because the two emission lines of OH share the same particular Einstein coefficient and total angular momentum, but the three emission lines of O_2 are located in different vibration bands with sufficiently different lower-state energy, which leads to a disparity in temperature sensitivity.

2.2 The $O_2(a^1\Delta_g)$ and OH dayglow limb radiance

In the case of limb-viewing, each viewing direction defines a ray path. The path segments defined by the intersection of atmospheric layers and ray paths is assumed to have the same emission and absorption characteristics. Evaluated on the layer-by-layer basis, the observed spectral irradiance is considered as a path integral along the line of sight[13]

$$L(\nu) = \int_{-\infty}^{\infty}\eta(s)D(\nu, s)\exp[-\int_{-s}^{\infty}n(s')\sigma(s')\mathrm{d}\,s']\mathrm{d}\,s \quad (3)$$

where $D(\nu)$ is the Doppler line shape of the spectral line, $\eta(s)$ is the volume emission rate $n(s)$ is the number density, $\sigma(s)$ is the absorption cross-section and s is the distance along the line-of-sight.

Figure 2 shows the limb spectral radiance of three emission lines of O_2 and the two emission lines of OH at different altitudes (40-90 km with 10 km interval). Inset shows a magnified view of a certain emission line, from which the linewidth and intensity varying with tangent heights can see more clearly.

The total spectral irradiance including the weak group of the O2 dayglow and the OH dayglow is shown in Fig. 3(a). ~~The total radiance including limb spectral radiance of the weak group of O_2 dayglow and the OH radiance is shown in Fig. 3. As can be seen,~~ ~~t~~The third emission line of the O_2 dayglow near 7823 cm^{-1} is too ~~closed~~ close to the OH lines $RR_{2.5e}$ and $RR_{2.5f}$ (less than 0.05 nm) to be well optically isolated. Figure 3(b) shows the band radiance profiles of the $O_2(a^1\Delta_g)$ near 7823 cm^{-1} and the OH dayglow, and their ratio. As can be seen, ~~T~~the OH dayglow~~radiance will surely~~ affects the observation of ~~spectral integral intensity of~~ the O_2 emission line near 7823 cm^{-1} especially for altitudes between 80 to 90 km where the OH radiance is relatively strong.

The Doppler shift of the emission line due to the movement of the atmosphere is measured as a phase shift of the Michelson interferometer, and accurate temperature measurement is obtained from the integrated absorbance ratio of two isolated emission lines [9]. However, the intensity variation caused by Doppler shift or temperature change is very small. The relative Doppler shift is w/c, where w denotes the motion of the background atmosphere and c is the velocity of light. If winds are to be measured to an accuracy of 3 m/s, a desirable value for the mesosphere and stratosphere, the measurement must be made

to one part in 10^8 of the velocity of light. For the central wavelength of 1270 nm, that means the measurement of the wavelength shift is about 12 fm (femtometre). Since a linewidth of the O_2 dayglow is of the order of 0.003 nm, the wavelength shift is 4×10^{-3} of the linewidth. Therefore, the intensity variation of the band radiance near 7823 cm^{-1} caused by the existence of the OH dayglow will surely contribute to the increase of wind error, as well as the temperature error.

3 Forward simulation

3.1 The instrument model

The NWTSI using the combination of a "strong" emission lines group and a "weak" group of the $O_2(a^1\Delta_g)$ airglow is a limb-viewing satellite instrument[9]. The schematic drawing of Limb-imaging geometry and Instrument concept is shown in Fig. 4, which closely follows the WAMI concept[6]. The field of view (FOV) of NWTSI is defined by the first telescope with a value of 1.5° × 1.5°, which allows NWTSI covering an entire altitude range from 20 to 120 km in single images for a nominal spacecraft altitude of 410 km.

The entrance aperture of NWTSI is about 5 cm in diameter with an effective aperture ratio of f/1.3. The magnifications of the first telescope and second are 2 and 0.5 respectively, so the FOV at the Michelson is 3° × 3° and at the filters is again 1.5° ×1.5°. The beam splitter of the NWTSI field-widened Michelson interferometer consists of two cemented half hexagons with a low-polarizing semi reflecting dielectric multilayer on one of the diagonal faces. It is made of BK7 glass and the entrance and exit faces are 6.35 cm^2. Large optical path difference (OPD) and field widening involve using 12.240 cm LaKN12 glass and 11.070 cm BK7 glass with corresponding refractive indices 1.733 and 1.516 in the two arms of the interferometer. The OPD between the paths of the two arms of the Michelson interferometer for normal incident can be found from $\Delta_0=2(n_1L_1-n_2L_2)$ [9], which corresponds to a value of 7.35 cm. In order to avoid errors caused by intensity variations during measurements, the four interferogram samples are taken simultaneously rather than sequentially by dividing one Michelson mirror into four equal segments so the steps are coated permanently onto the mirror. A composite of etalon and interference filter is used to isolate individual emission lines. The etalon is fused silica with a finesse of 20 and a free spectral range of 2.0 nm. The etalon thickness is designed to give optimum transmittance in the outer one-third of the field of view for three strong/weak O2 emission lines. The imaging system produces four copies of FOV by using a shallow, pyramid shaped prism just in front of the camera. The edges of the prism are aligned with the divisions between the quadrants of the sectored Michelson mirror to form 4 images on the array detectors simultaneously, corresponding different sampling steps of the Michelson segments.

3.2 The imaging interferogram

By sampling the interferogram for each pixel at four points corresponding to the four phase steps, the Doppler wind is obtained, which is so called the four-point sampling method. The equation representing the interferogram for a given pixel at row *l* and column *j* of the detector is[14]

$$I_{klj} = R_{lj}\int_{\nu_1}^{\nu_2} f_{lj}(\nu)\cdot L_{lj}(\nu)\cdot\left[1+U_{lj}\cos(2\pi\nu\Delta_{lj}+\varphi_{klj})\right]d\nu \tag{4}$$

where $f_{lj}(\nu)$ is the relative total filter function, U_{lj} is the instrument visibility, Δ_{lj} is the OPD, and φ_{klj} is the Michelson interferometer *k*th phase step, ν is the wavenumber, the instrument responsivity R_{lj} is defined by

$$R_{lj} = \frac{A\Omega t\tau q}{hc\nu_0} \tag{5}$$

where $A\Omega$ is the Pixel etendue, t is the Exposure time, τ is the attenuation, q is the quantum efficiency.

The simulated mean value of the interferogram for the weak group of O_2 dayglow as well as the OH radiance is shown in Fig. 5. The pattern on Fig. 5(a) reflects the variation over the field of the filter transmittance function, the dependence of ~~optical path difference~~OPD on pixel positions, and the tangent height variation of O_2 dayglow within a column. The image in Fig. 5(b) shows the interference fringe of OH radiance is much stronger for pixels nearer the periphery of focal plane array (FPA)~~FPA~~, where the signal of the third weak emission line of the O_2 dayglow near 7823 cm^{-1} is imaged.

4 Inversion error due to the effect of OH radiance

Molecular species in NWTSI's selected spectral range of 7820-7824 cm^{-1} and 7908-7912 cm^{-1} other than O_2 can affect NWTSI's wind and temperature measurements through absorption and emission. Limb spectral radiance of OH airglow is the most important interfering constituents for NWTSI, especially for the "weak" group detection, as shown in Fig. 3 and Fig. 5. Using etalon as the ultra-narrow filter significantly reduces but does not eliminate the influence from OH airglow. Therefore, the uncertainty in its mixing ratio surely contributes to the increase of wind and temperature errors. Note that while the fabrication of this ultra-narrow filter with a spectral width of 0.1 nm is feasible for current technical level and engineering capability, it would be extremely challenging to monitor the changes in its width and central wavelength during the duration of the mission.

The wind velocity v_w is measured as a phase shift $\delta\varphi$ of the interferogram

$$v_w = \frac{c}{2\pi\Delta\nu_0}\delta\varphi \tag{6}$$

And phase φ can be calculated from:

$$\varphi_t = \tan^{-1}\left(\frac{J_3}{J_2}\right) \tag{7}$$

Fourier coefficients, J_1, J_2, and J_3, also referred to as the apparent quantities, are related to any point k along a fringe interferogram I [2]:

$$\begin{aligned} J_1 &= I_{mean} = \frac{1}{4}\sum_{k=1}^{4} I_k \\ J_2 &= \frac{1}{2U}\sum_{k=1}^{4} I_k \cos(\varphi_{klj}) \\ J_3 &= \frac{1}{2U}\sum_{k=1}^{4} I_k \sin(\varphi_{klj}) \end{aligned} \tag{8}$$

Omitting the presence of OH emission will change the value of J_2 and J_3, which will inevitably lead to an inversion error for the wind measurement. ~~The contribution of OH radiance to the wind error is shown in Fig. 6(a). As can be seen, the wind error is about 1-2 m/s for altitudes below 70 km, climbing to greater than 8 m/s as the altitude increases from 80 to 90 km. The sensitivity of wind retrieval is weaker in the lower altitudes due to lower OH volume emission rate. A similar trend is found for the temperature obtained from J_1: the temperature error is about 4-6 K for altitudes below 70 km and greater than 20 K for altitudes from 80 to 90 km (see Fig. 6(b)). By happy coincidence, the wind and temperature inversion for altitude above 70 km is irrelevant to the "weak" group. The three strong emission lines suffering little from self-absorption at relatively higher tangent heights takes the place of the weak group for data inversion.~~

The error standard deviation of inverted wind due to the presence of OH emission is found from the relation[9]:

$$\sigma_v = c\,\frac{\sqrt{J_2^2\sigma_{J_3}^2 + J_3^2\sigma_{J_2}^2}}{2\pi\nu_0\Delta(J_2^2+J_3^2)} \quad (9)$$

Where $\sigma_{J_2}^2$ and $\sigma_{J_3}^2$ represents the variance of the Fourier coefficients J_2 and J_3 due to the lack of knowledge on OH emission.

The contribution of OH dayglow to the wind error is shown in Fig. 6(a). The black curve represents omitting the presence of the OH emission. As can be seen, the wind error is about 1-2 m/s for altitudes below 70 km, climbing to greater than 8 m/s as the altitude increases from 80 to 90 km. The sensitivity of wind retrieval is weaker in the lower altitudes due to lower OH volume emission rate. The degree of knowledge of OH dayglow is important for NWTSI retrieval. The blue short dash dot and the red short dash in Fig. 6(a) represent the errors deviation of inverted wind with OH dayglow knowledge of 80 % and 90 %, respective. As can be seen, when OH dayglow is known to 80%, the wind error is 0.3–0.5 m/s for the altitude range of 40–70 km; for OH dayglow knowledge of 90%, the wind error decreases to 0.1–0.3 m/s m.

The error standard deviation of inverted temperature due to the presence of OH emission can be written as

$$\sigma_T = \frac{\Delta T}{T} = \frac{R_{AB}}{T}\frac{dT}{dR_{AB}}\sqrt{\sigma_{J_{1A}}^2 + \sigma_{J_{1B}}^2} \quad (10)$$

Where $\sigma_{J_{1A}}^2$ and $\sigma_{J_{1B}}^2$ represent the variance of the Fourier coefficients J_1 of two emission lines *A* and *B* of the weak group of the O_2 dayglow, and R_{AB} is the ratio of the measured integral absorbances of this two lines, $R_{AB} = J_{1A}/J_{1B}$. ~~The effect of OH airglow on wind and temperature inversion can be reduced by excluding the tainted data pixels or improving OH radiance knowledge. The first option is infeasible for NWTSI because the weak emission line tainted by the OH airglow has the largest spatial coverage. Another option is to retrieve OH radiance. This option might potentially improve OH radiance knowledge to a very limited degree (depending on the uncertainty of the initial guess), and resulting OH radiance error will also be introduced by the retrieval to compensate for other error sources that are not well accounted for.~~

~~The degree of knowledge of OH radiance is important for NWTSI retrieval. Fig. 7 shows the errors deviation of inverted wind and temperature with OH radiance knowledge of 80 % and 90 %. As can be seen, when OH radiance is known to 80%, the wind error is 0.3–0.5 m/s and temperature error is 0.7–1.0 K for the altitude range of 40–70 km; for OH radiance knowledge of 90%, the wind error decreases to 0.1–0.3 m/s m and temperature error decreases to 0.3–0.5 K.~~

A similar trend with the wind error is found for the temperature obtained from J_{1A} and J_{1B}: the temperature error is about 4-6 K for altitudes below 70 km and greater than 20 K for altitudes from 80 to 90 km (see the black curve in Fig. 6(b)). When OH dayglow is known to 80%, the temperature error is 0.7-1.0 K for the altitude range of 40–70 km (see the blue short dash dot in Fig. 6(b)); for OH dayglow knowledge of 90%, the temperature error decreases to 0.3-0.5 K (see the red short dash in Fig. 6(b)).

By happy coincidence, the wind and temperature inversion for altitude above 70 km is irrelevant to the "weak" group. Due to their relative weak self-absorption effect, the weak emission lines are used only for wind and temperature measurement at low altitude. The three strong emission lines suffering little from self-absorption at relatively higher tangent heights takes the place of the weak group for data inversion.

The performance analyses presented assume that the OH radiance is known to a degree that results in meeting the threshold wind and temperature accuracies. The largest errors are obtained when not accounting for OH radiance in the retrievals. In order to ~~ring~~ bringdown the wind and temperature error to an acceptable level, OH radiance knowledge with an accuracy of 80-90 % is required.

5 Conclusions

We have simulated and discussed the effect of OH radiance on the wind and temperature measurements derived from the 1.27 μm O_2 dayglow limb-viewing observations. We first calculated the O_2 ~~dayglow~~ and OH dayglow ~~radiance~~ spectrum over the

spectral region and altitude range of interest using the line-by-line radiative transfer model and the photochemical model incorporating the most recent spectroscopic parameters, rate constants and solar fluxes. Its shows that the OH lines $RR_{2.5e}$ and $RR_{2.5f}$ is too ~~closed~~close to the third weak emission line of the O_2 dayglow near 7823 cm^{-1} (less than 0.05 nm), which will surely affect the spectral integral intensity of the O_2 mission line. A brief description of the instrument model of NWTSI including the schematic drawing of Limb-imaging geometry and the instrument concept is presented. The method of four-point sampling of the interferogram and sample results of measurement simulations are provided for both O_2 ~~dayglow~~ and OH dayglow~~radiance~~. It was apparent from the simulations that the interference fringe of OH radiance is much stronger for pixels nearer the periphery of FPA, where the signal of the third weak emission line of the O_2 dayglow near 7823 cm^{-1} is imaged. Inversion errors of wind and temperature measurements due to the effect of OH radiance are presented and discussed in detail. The presence of OH radiance as an interfering species decreases the NWTSI performance at all altitudes with the largest impact especially for altitudes from 80 to 90 km. The effect of OH airglow on NWTSI inversion can be reduced by improving OH radiance knowledge. Accurate $OH(v=8)$ concentrations (uncertainty level of 20 % or better) are required to help meet the wind and temperature accuracy requirements.

Code availability. Available upon request.

Author contribution. Kuijun Wu and Weiwei He conceived the ideas, developed the forward model, performed the measurement simulation, and wrote the manuscript. Yutao Feng helped in the instrument concept and error analysis. Yuanhui Xiong calculated the atmospheric limb radiance. Faquan Li provided optical design expertise knowledge. All the authors contributed to the analysis and discussion of the results.

Acknowledgments. This work was supported by National Natural Science Foundation of China (NSFC) (41975039, 61705253) and National Key R&D Program of China (2017YFC0211900). The authors gratefully acknowledge informative and helpful discussions with Wang Dingyi on theoretical details of this work.

References

1. M. G. Mlynczak, B. T. Marshall, F. J. Martin-Torres, J. M. Russell, R. E. Thompson, E. E. Remsberg, and L. L. Gordley, "Sounding of the Atmosphere using Broadband Emission Radiometry observations of daytime mesospheric $O_2(a^1\Delta_g)$ 1.27 μm emission and derivation of ozone, atomic oxygen, and solar and chemical energy deposition rates," J. Geophys. Res. Atmos. 112(D15), D15306 (2007).
2. G. G. Shepherd, G. Thuillier, Y. M. Cho, M. L. Duboin, W. F. J. Evans, W. A. Gault, C. Hersom, D. J. W. Kendall, C. Lathuillere, R. P. Lowe, I. C. McDade, Y. J. Rochon, M. G. Shepherd, B. H. Solheim, D. Y. Wang, and W. E. Ward, "The Wind Imaging Interferometer (WINDII) on the Upper Atmosphere Research Satellite: A 20 Year Perspective," Rev. Geophys. 50(2), 713–723 (2012).
3. D. A. Ortland, W. R. Skinner, P. B. Hays, M. D. Burrage, R. S. Lieberman, A. R. Marshall, and D. A. Gell, "Measurements of stratospheric winds by the high resolution Doppler imager," J. Geophys. Res. Atmos. 101(D6), 10351-10363 (1996).
4. T. L. Killeen, Q. Wu, S. C. Solomon, D. A. Ortland, W. R. Skinner, R. J. Niciejewski, and D. A. Gell, "TIMED Doppler Interferometer: Overview and recent results," J. Geophys. Res. Space 111, A10S01 (2006)

5. K. J. Wu, D. Fu, Y. T. Feng, J. Li, X. B. Hao, and F. Q. Li, “Simulation and application of the emission line $O_{19}P_{18}$ of $O_2(a^1\Delta_g)$ dayglow near 1.27 μm for wind observations from limb-viewing satellites,” Opt. Express 26(13), 16984-16999 (2018).
6. W. E. Ward, W. A. Gault, G. G. Shepherd, and N. Rowlands, “The Waves Michelson Interferometer: A visible/near-IR interferometer for observing middle atmosphere dynamics and constituents,” Proc. SPIE 4540, 100–111 (2001).
7. W. E. Ward, W. A. Gault, N. Rowlands, S. Wang, G. G. Shepherd, I. C. McDade, J. C. McConnell, D. Michelangeli, and J. Caldwell, "An imaging interferometer for satellite observations of wind and temperature on Mars, the Dynamics Atmosphere Mars Observer (DYNAMO)," Applications Of Photonic Technology 5 4833, 226-236 (2002).
8. R. Zhang, W. E. Ward, and C. M. Zhang, "O_2 nightglow snapshots of the 1.27 μm emission at low latitudes on Mars with a static field-widened Michelson interferometer," J. Quant. Spectrosc. Radiation 203, 565–571 (2017).
9. W. He, K. Wu, Y. Feng, D. Fu, Z. Chen, and F. Li, "The Near-Space Wind and Temperature Sensing Interferometer: Forward Model and Measurement Simulation," Remote Sens-Basel **11**, 914 (2019).
10. T. Maihara, F. Iwamuro, T. Yamashita, D. N. B. Hall, L. L. Cowie, A. T. Tokunaga, and A. Pickles, " Observations of the OH airglow emission," Publ. Astron. Soc. Pac. 105, 940-944 (1993).
11. M. G. Mlynczak, S. Solomon, and D. S. Zaras, “An updated model for $O_2(a^1\Delta_g)$ concentrations in the mesosphere and lower thermosphere and implications for remote-sensing of Ozone at 1.27 μm,” J. Geophys. Res. Atmos. 98(D10), 18639–18648 (1993).
12. J. P. Russell and R. P. Lowe, "Atomic oxygen profiles (80-94 km) derived from Wind Imaging Interferometer/Upper Atmospheric Research Satellite measurements of the hydroxyl airglow: 1. Validation of technique," J. Geophys. Res. 108(D21), 4662 (2003).
13. R. Song, M. Kaufmann, J. Ungermann, M. Ern, G. Liu, and M. Riese, “Tomographic reconstruction of atmospheric gravity wave parameters from airglow observations,” Atmos. Meas. Tech. 10, 4601-4612 (2017).
14. P. Rahnama, Y. J. Rochon, I. C. Mcdade, G. G. Shepherd, W. A. Gault, and A. Scott, “Satellite Measurement of Stratospheric Winds and Ozone Using Doppler Michelson Interferometry. Part I: Instrument Model and Measurement Simulation,” J. Atmos. Ocean. Tech. 23, 753-769 (2006).

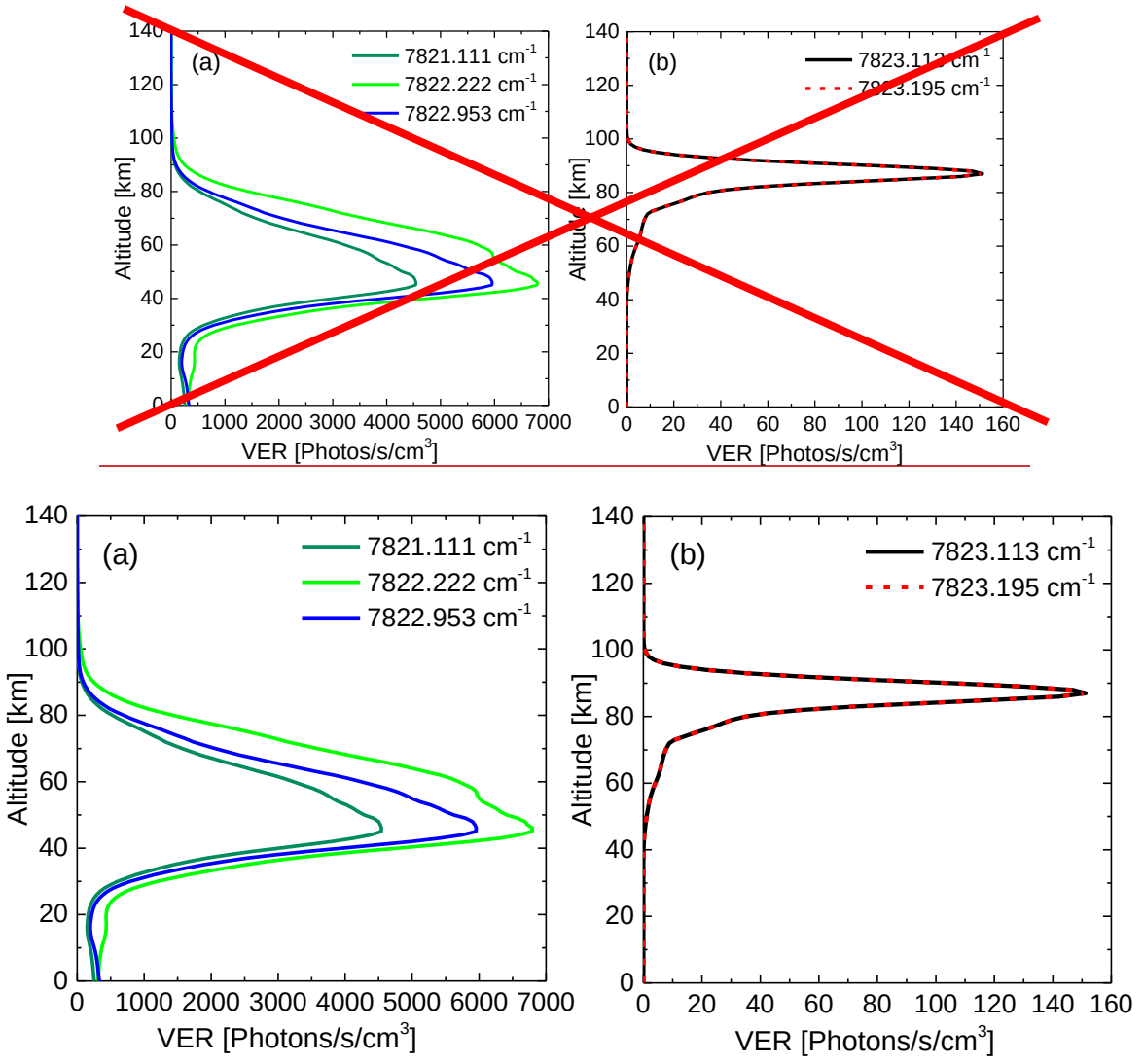

Figure. 1: The VER profiles of both the three weak target emission lines of the 1.27 μm O_2 dayglow and the two emission lines of OH.

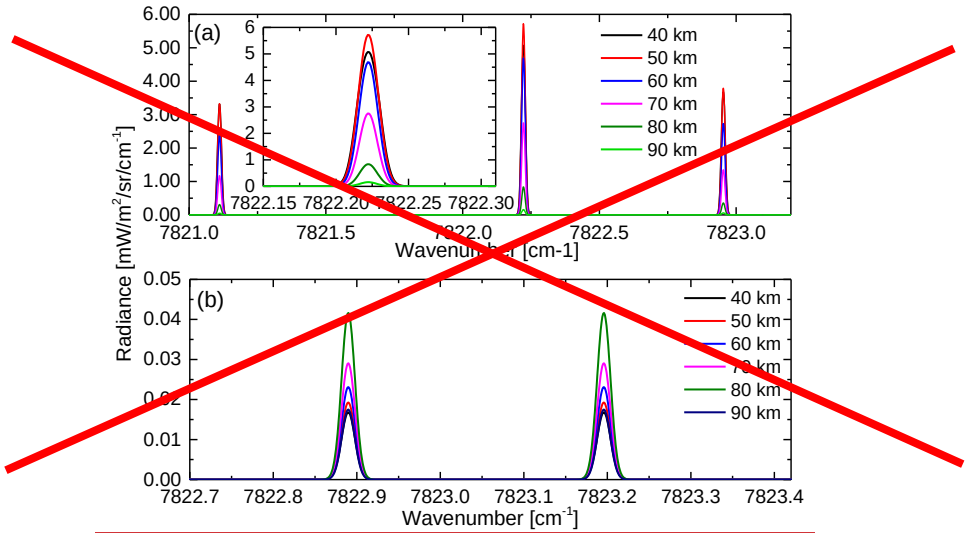

~~Figure. 2: The emission spectra of the three emission lines of O2 dayglow and the two emission lines of OH at tangent heights of 40 km, 50 km, 60 km, 70 km, 80 km and 90 km.~~

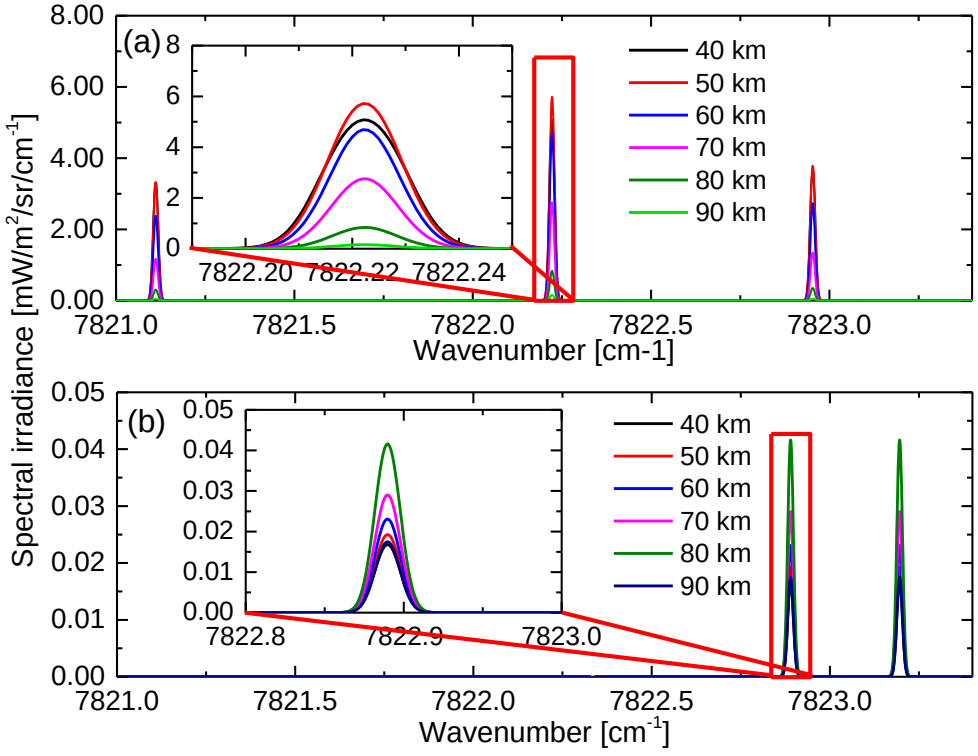

Figure. 2: The spectral irradiance of the three emission lines of O_2 dayglow and the two emission lines of OH dayglow at tangent heights of 40 km, 50 km, 60 km, 70 km, 80 km and 90 km. (a) three emission lines of O_2 dayglow. (b) two emission lines of OH dayglow. Inset to (a) or (b) shows a magnified view of a certain emission line of O_2 or OH dayglow, from which the linewidth and intensity varying with tangent heights can see more clearly.

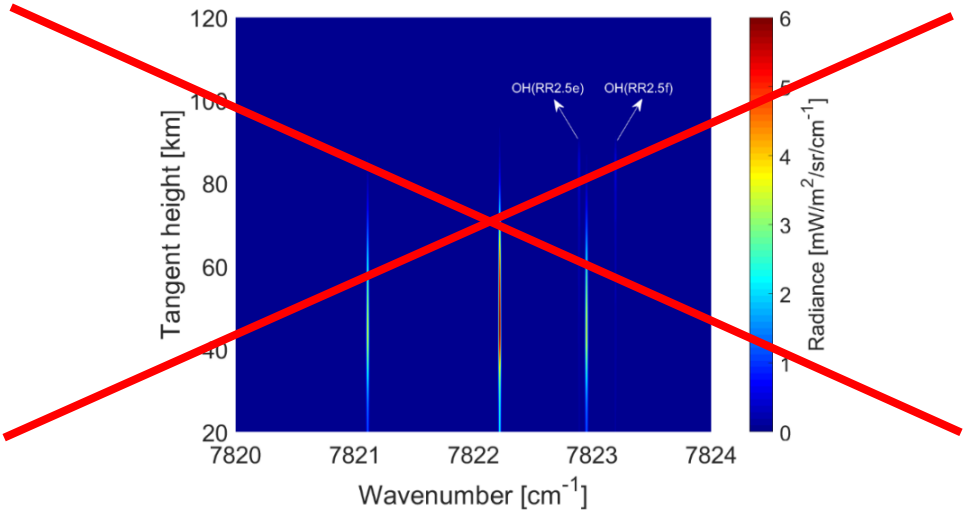

295

~~**Figure. 3: The total spectral radiance containing $O_2(a^1\Delta_g)$ and OH dayglow as a function of tangent height.**~~

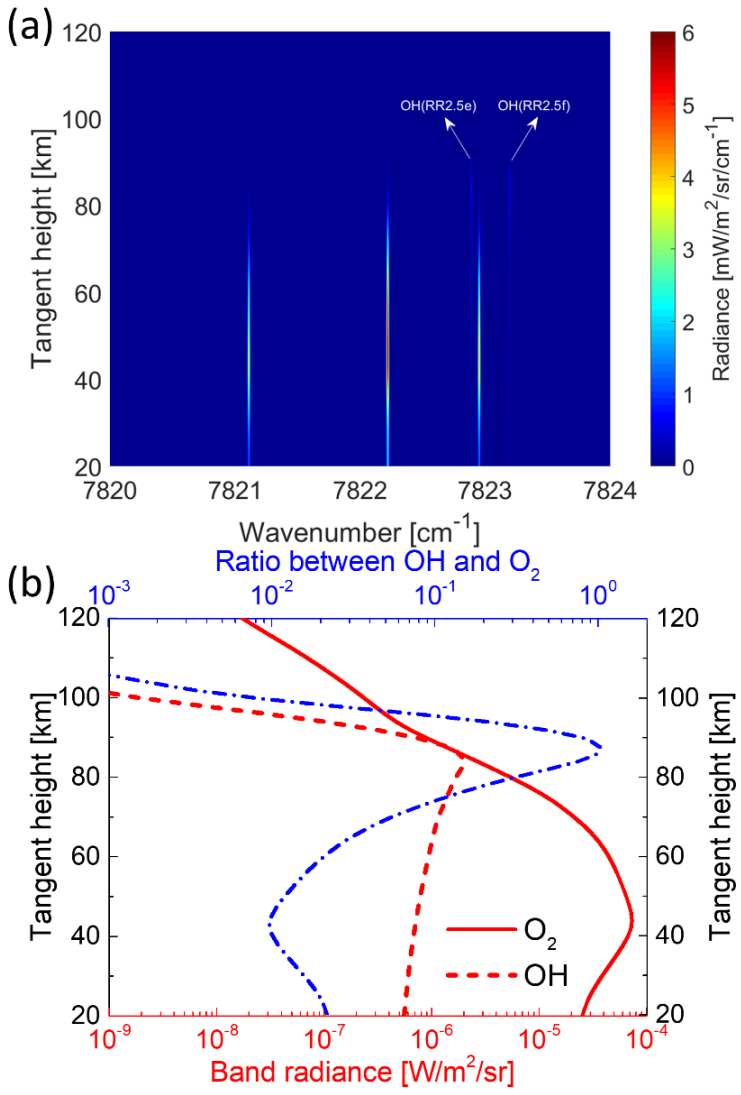

Figure. 3: The total spectral irradiance and band radiance as a function of tangent height. (a) the total spectral irradiance containing $O_2(a^1\Delta_g)$ and OH dayglow as a function of tangent height. (b) the band radiance profiles of the $O_2(a^1\Delta_g)$ and OH dayglow and their ratio.

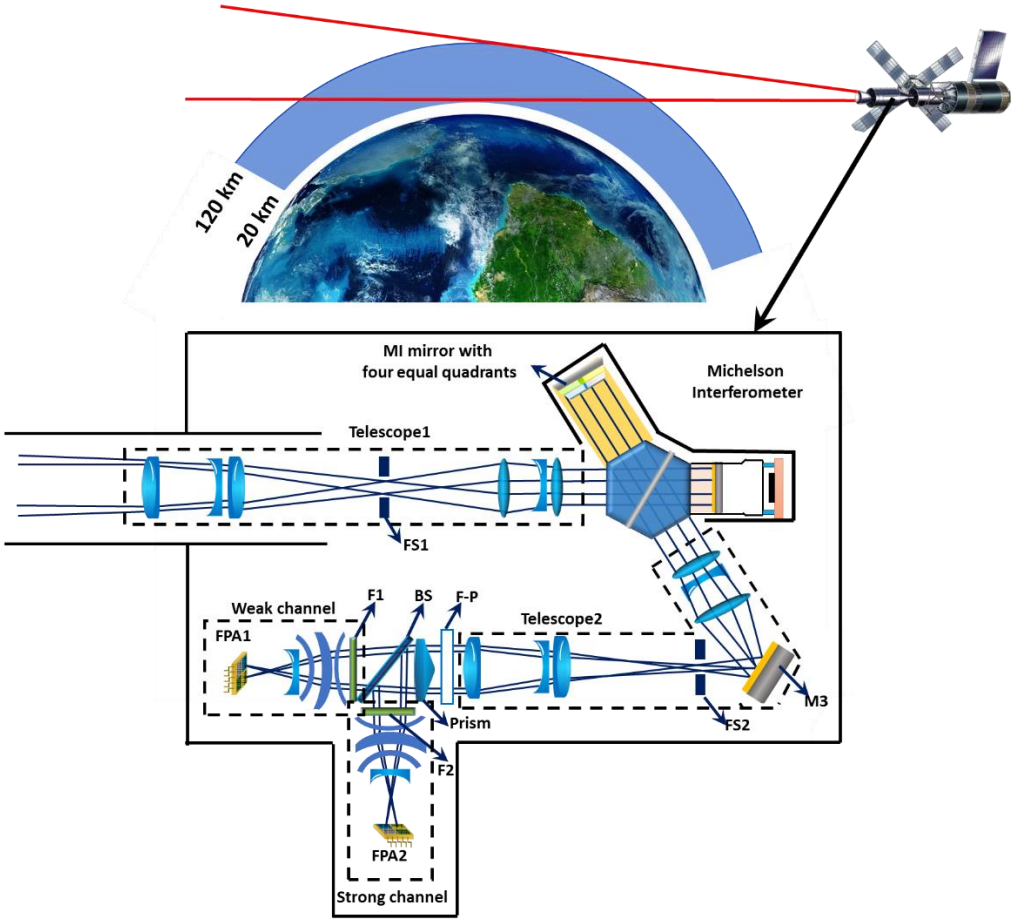

Figure. 4: Limb-imaging geometry and optical concept schematic drawing for NWTSI.

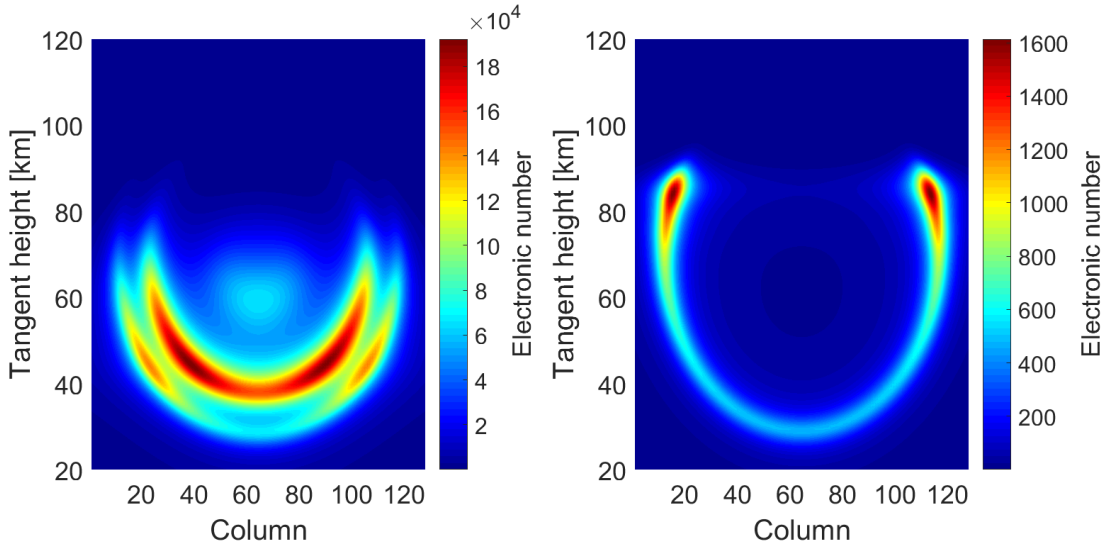

Figure. 5: The simulated interferogram images of the weak $O_2(a^1\Delta_g)$~~O2(a1Δg)~~ and OH emission lines.

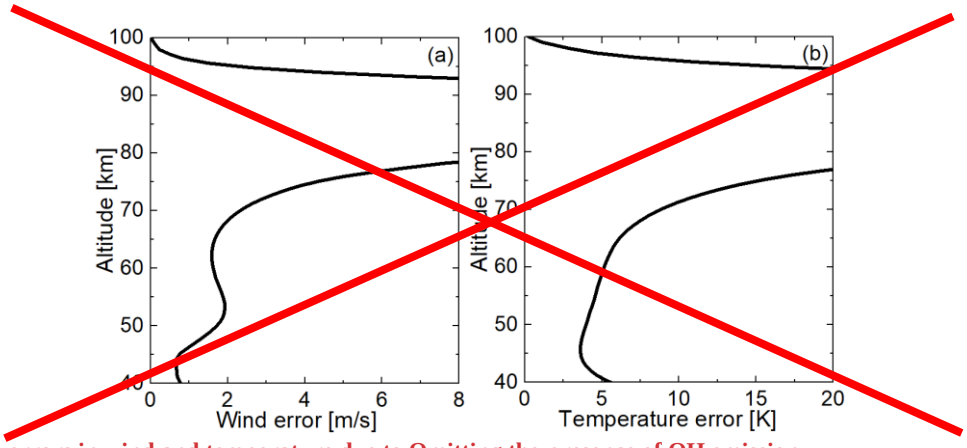

~~Figure. 6: Inversion errors in wind and temperature due to Omitting the presence of OH emission.~~

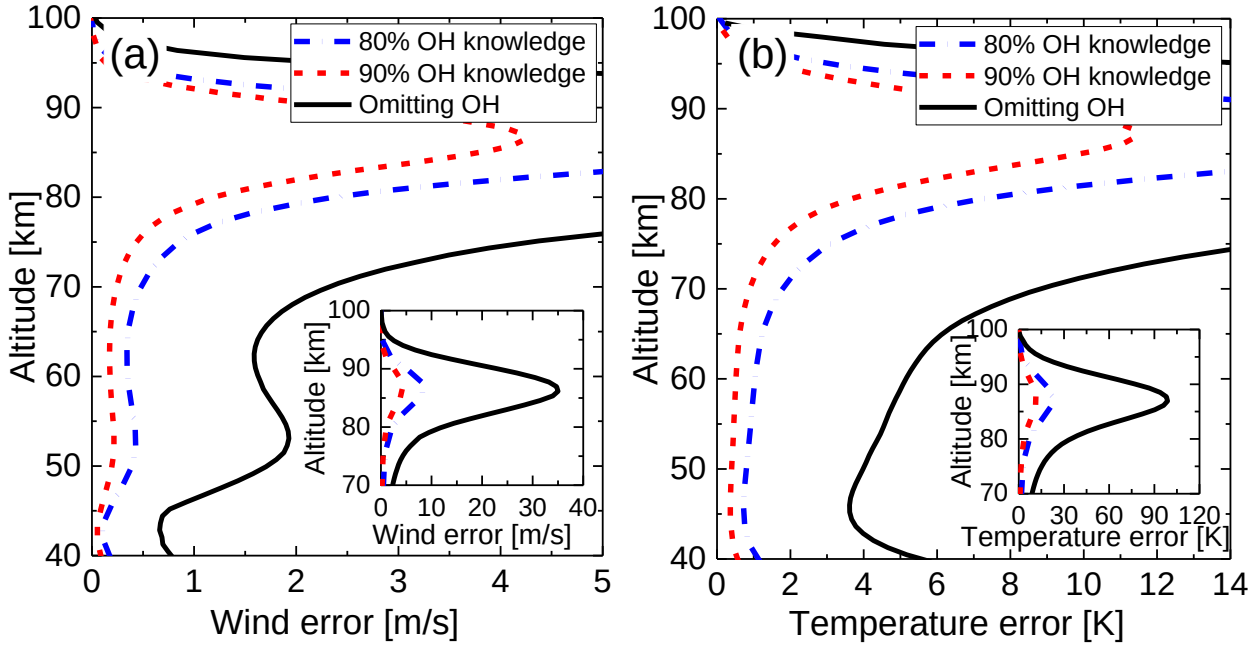

Figure. 6: Inversion errors in wind and temperature due to omitting the presence of OH dayglow (black curve) and with 80% and 90% knowledge of the OH dayglow (blue short dash dot and the red short dash). (a) the wind error profiles. (b) the temperature error profiles. Inset to (a) or (b) shows the wind or temperature error in the altitude range 70-100 km.

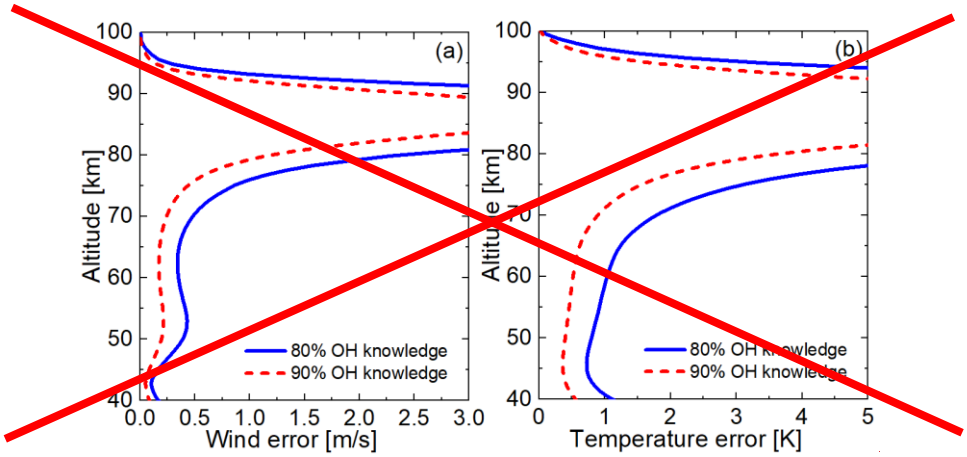

Figure. 7: Inversion errors in wind and temperature with 80% and 90% knowledge of the OH radiance.

315